

# Building Facade Point Clouds Segmentation Based on Optimal Dual-Scale Feature Descriptors

Zijian Zhang, Jicang Wu

College of Surveying and Geo-Informatics, Tongji University, Shanghai, China  
Email: zhangzijian@tongji.edu.cn

**How to cite this paper:** Zhang, Z.J. and Wu, J.C. (2024) Building Facade Point Clouds Segmentation Based on Optimal Dual-Scale Feature Descriptors. *Journal of Computer and Communications*, 12, 226-245.

<https://doi.org/10.4236/jcc.2024.126014>

**Received:** June 2, 2024

**Accepted:** June 25, 2024

**Published:** June 28, 2024

---

## Abstract

To address the current issues of inaccurate segmentation and the limited applicability of segmentation methods for building facades in point clouds, we propose a facade segmentation algorithm based on optimal dual-scale feature descriptors. First, we select the optimal dual-scale descriptors from a range of feature descriptors. Next, we segment the facade according to the threshold value of the chosen optimal dual-scale descriptors. Finally, we use RANSAC (Random Sample Consensus) to fit the segmented surface and optimize the fitting result. Experimental results show that, compared to commonly used facade segmentation algorithms, the proposed method yields more accurate segmentation results, providing a robust data foundation for subsequent 3D model reconstruction of buildings.

## Keywords

3D Laser Scanning Point Clouds, Building Facade Segmentation, Point Cloud Processing, Feature Descriptors

---

## 1. Introduction

With the development of LiDAR (Light Detection and Ranging) technology and the advancement of the “smart city” concept, constructing LoD (Level of Detail) models of urban buildings using ground laser scanning systems has become a research hotspot among scholars both domestically and internationally. Ground LiDAR systems are widely used in urban 3D modeling due to their advantages of fast data acquisition, high precision, and non-contact measurement. These systems are also one of the key methods for data acquisition in the field of 3D modeling [1]-[3].

The primary facade of a building refers to the continuous surface in the building's point clouds that contains the most points. This surface is usually a wall without windows, representing the basic form of the building and serving as a key basis for constructing the building's LoD model. Extracting the primary facade is a prerequisite for building the LoD model. Accurately segmenting the primary facade of a building based on ground laser scanning systems is currently a significant research challenge. For most buildings, their structure is a simple planar form, meaning that the building is composed of four faces. For these types of buildings, a single surface fitting can yield the primary facade. However, for more complex buildings, the facade is composed of multiple intersecting planar segments. A single surface fitting cannot capture all the walls, leading to structural omissions and consequently affecting the accuracy of the subsequent LoD model. To address this issue, it is necessary to segment the building facade point clouds to precisely extract the primary facade [4].

The purpose of point clouds segmentation is to divide point clouds data into multiple homogeneous regions, where the points within the same region have similar or identical features (such as normal vectors, curvature, etc.). Currently, segmentation based on point clouds, both domestically and internationally, primarily focuses on the local neighborhood characteristics and geometric features of the point clouds [5]-[8]. Wang Y *et al.* proposed an urban point clouds segmentation method based on Gaussian maps. This method maps the normal vectors of the point clouds to a Gaussian map and clusters them, then groups the clustering results to identify planes, cylinders, and other shapes in the scene. However, relying solely on normal vectors results in point clouds with similar normal vectors being classified into the same category, failing to achieve refined segmentation results [9]. Wang W *et al.* implemented the segmentation of indoor building scenes based on an improved RG (RG) algorithm. This approach enhances traditional RG performance through more accurate normal vector estimation and strengthened RG criteria. However, for different datasets, the method still requires adjusting the normal vector angle and curvature thresholds, lacking a more universal threshold reference value [10]. Jampani V *et al.* converted facade point clouds into facade images and performed classification based on the pixels in the image. This method is simple and efficient, effectively transforming the point clouds segmentation problem into an image classification problem. However, the method becomes less applicable when building facades are complex [11].

Based on the aforementioned research, the current issues in the field of building facade point clouds segmentation can be summarized as follows: 1) poor segmentation accuracy; 2) low applicability of segmentation methods; and 3) lack of universal parameter threshold references. To address these issues, we propose a method (ODSFD) for extracting building primary facades based on optimal dual-scale feature descriptors. ODSFD first utilizes public datasets and simulated data to select the optimal dual-scale descriptors from numerous proposed feature descriptors, providing key threshold values as general references

for users. Next, a facade segmentation algorithm is constructed based on the proposed dual-scale descriptors. Finally, experiments are conducted using self-collected data to verify the accuracy and feasibility of ODSFD. According to the final quantitative results, the proposed method not only achieves high segmentation accuracy but is also applicable to complex building facades composed of multiple small patches.

## 2. Methodology

### 2.1. Research Objective

The ODSFD we propose for extracting building primary facades is based on the features of points. The feature descriptor of a point clouds is a digital representation of the point's geometric characteristics. Points with different attributes possess distinct features. As shown in **Figure 1**, regular points (RP) represent the planar parts of the point clouds, while sharp points (SP) represent the points where different planes intersect. Therefore, distinguishing between regular and sharp points enables the segmentation of different planes.

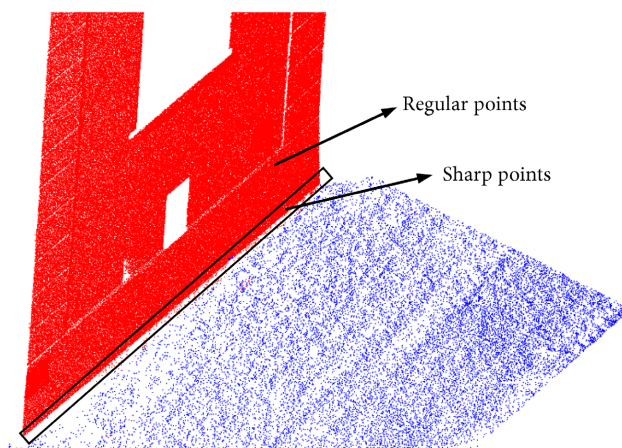


**Figure 1.** The diagram of regular points and sharp points.

### 2.2. Feature Descriptors of Point Clouds

To distinguish between regular and sharp points, we generate feature descriptors based on eigenvalues. These descriptors effectively characterize the regular or sharp features of points, such as linearity, planarity, sphericity, anisotropy, eigenentropy, omnivariance, surface variation, and verticality. Depending on the geometric significance of the feature descriptors, they can be classified into two categories: dimensional feature descriptors and statistical feature descriptors. These descriptors are crucial for distinguishing between regular and sharp points and are widely used in current geometric feature analysis [12] [13]. To compute these descriptors, we first calculate the eigenvalues of the points. The eigenvalues of a point  $P_i$  are typically derived from the covariance matrix of all points within a specified radius around the point. We calculate the eigenvalues of the point clouds based on PCA (Principal Component Analysis) [14] [15], expressed as

Equation (1):

$$Q_p = \frac{1}{N} \sum_{i=1}^N (P_i - \bar{P})(P_i - \bar{P})^T. \quad (1)$$

where,  $Q_p$  represents the covariance matrix of all points within a certain radius of point  $P_i$ ;  $N$  is the total number of points in this neighborhood,  $i = 1, 2, \dots, N$ ;  $\bar{P}$  is the mean of all points in the neighborhood, and it can be expressed as Equation (2):

$$\bar{P} = \frac{1}{N} \sum_{i=1}^N P_i. \quad (2)$$

Based on the covariance matrix, we can calculate the eigenvalues of point  $P_i$  and further obtain its feature descriptors. The expressions for each descriptor are as **Table 1**:

**Table 1.** Expression of feature descriptors.

Feature Descriptors	Formula	Style
$L_{\text{linearity}}$	$(\lambda_1 - \lambda_2)/\lambda_1$	Dimensional Feature
$P_{\text{planarity}}$	$(\lambda_2 - \lambda_3)/\lambda_1$	
$S_{\text{sphericity}}$	$\lambda_3/\lambda_1$	
$A_{\text{anisotropy}}$	$(\lambda_1 - \lambda_3)/\lambda_1$	Statistical Feature
$E_{\text{eigenentropy}}$	$-\sum_{i=1}^3 \lambda_i \ln(\lambda_i)$	
$O_{\text{omnivarience}}$	$(\lambda_1 \cdot \lambda_2 \cdot \lambda_3)^{1/3}$	
$S_{\text{surface\_variation}}$	$\lambda_3/(\lambda_1 + \lambda_2 + \lambda_3)$	
$V_{\text{verticality}}$	$1 - \left\langle [0 \ 0 \ 1], \vec{e}_3 \right\rangle$	

where,  $L_{\text{linearity}}$  represents the linearity of point;  $P_{\text{planarity}}$  represents the planarity of point;  $S_{\text{sphericity}}$  represents the sphericity of point;  $A_{\text{anisotropy}}$  represents the anisotropy of point;  $E_{\text{eigenentropy}}$  represents the eigenentropy of point;  $O_{\text{omnivarience}}$  represents the omnivarience of point;  $S_{\text{surface\_variation}}$  represents the surface variation of point;  $V_{\text{verticality}}$  represents the verticality of point;  $\lambda_1, \lambda_2, \lambda_3$  represent the normalized eigenvalues of point, and  $\lambda_1 \geq \lambda_2 \geq \lambda_3$ ;  $\vec{e}_3$  represent the eigenvectors corresponding to the smallest eigenvalue  $\lambda_3$ .

Although these descriptors have certain capabilities to characterize the sharpness of points, experimental verification and analysis are still needed to determine which descriptors are more effective in distinguishing between regular and sharp points. For instance, linearity represents the linear characteristics of points in their neighborhoods, such as the point clouds of lampposts in urban areas, which tends to have a linearity close to 1. Planarity and anisotropy represent the planar characteristics of points in their neighborhoods, such as the planarity of building facades, which tends to be close to 1. Sphericity represents the degree of

dispersion of points in their neighborhoods, such as the high sphericity of points in a tree leaf point clouds. Eigenentropy, omnivariance, surface variation, and verticality can all predict the position of points in the entire point set.

Under normal circumstances, multi-scale descriptors have better sharp point extraction performance compared to single descriptor. However, when the difference in accuracy is not significant, multi-scale computation can significantly increase algorithm complexity and computational costs [16]. Therefore, to reduce algorithm complexity and provide reference values, we analyze and select two descriptors through experiments to form optimal dual-scale descriptors.

### 2.3. Segmentation Algorithm of ODSFD

Assuming that the obtained optimal dual-scale feature descriptors are  $D_1$  and  $D_2$ , and their threshold reference values are  $v_1$  and  $v_2$  respectively, we can use these dual-scale descriptors and their reference values to distinguish between regular and sharp points in the point clouds and construct the ODSFD algorithm. The ODSFD is based on the traditional RG algorithm, but unlike the traditional RG algorithm, the threshold values of its two key parameters usually remain constant across different datasets. The ODSFD steps are as follows:

- 1) For the point clouds to be segmented, sort the points based on their  $D_1$  values, and select the point with the minimum  $D_1$  as the initial seed point. Add this initial seed point to the seed point set;
- 2) Calculate the difference of  $D_2$  between each neighboring point of the seed point and the seed point. If the difference is less than  $v_2$ , classify the neighboring point and reevaluate the difference between its  $D_1$  value and the seed point's  $D_1$ . Otherwise, do not classify the neighboring point;
- 3) If the difference of  $D_1$  is less than  $v_1$ , add the neighboring point to the seed point set; otherwise, classify the neighboring point but do not add it to the seed point set;
- 4) Remove the current seed point from the seed point set and continue to "grow" with the new seed point, repeating steps b) to c). Continue this process until the seed point set is empty, indicating that the growth of this class is complete. All classified points form one class;
- 5) For the remaining unclassified points, repeat steps a) to d) until all points are classified.

However, due to the complexity of real building structures or the incomplete accuracy of the given empirical parameters, over-segmentation issues still exist. The RANSAC algorithm, one of the most common algorithms in point clouds fitting, not only provides a good plane fitting effect but also offers better noise resistance compared to least squares fitting. To address the over-segmentation problem, this paper proposes the following optimization methods and constraints based on the RANSAC algorithm for fitting the segmentation results [17] [18]. The schematic diagram is shown in **Figure 2**:

- 1) For each segmented point sets  $S = \{S_1, S_2, \dots, S_n\}$  perform plane fitting using the RANSAC;

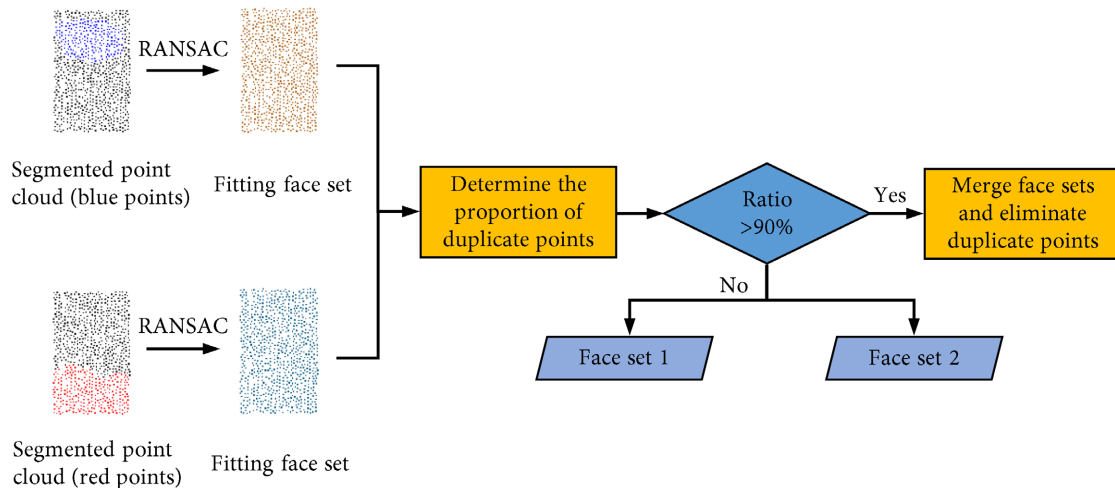


**Figure 2.** The optimization method of ODSFD.

2) For point set  $S_i$ , extract all points from the original point set that are within 0.05 m of the fitted plane and designate this point set as a new set  $C_i$ .  $C_i$  may contain points that are in the same plane as  $S_i$  but belong to different classes;

3) Use the DBSCAN (Density-Based Spatial Clustering of Applications with Noise) algorithm to segment point set  $C_i$  and obtain point sets  $G = \{G_1, G_2, \dots, G_m\}$  [19] [20]. From point set  $G = \{G_1, G_2, \dots, G_m\}$ , select the point set whose centroid is closest to a distance  $S_i$  from the centroid. This point set represents the set of face in the original point clouds corresponding to the segmented point set  $S_i$ ;

4) After all segmented point sets  $S = \{S_1, S_2, \dots, S_n\}$  have been fitted, determine if the number of duplicate points between any two sets of faces is greater than 90% of the total number of points in the set with fewer points. If so, merge the points within the two faces, and delete duplicate points until no more faces can be merged.

By using the above method, not only has the over-segmentation problem in the segmentation process been improved, but also the robustness of the ODSFD algorithm has been enhanced. Additionally, further denoising of the point clouds has been achieved.

### 3. Experiments and Analysis

We designed three experiments to select the optimal dual-scale descriptors and validate the feasibility of the ODSFD. These experiments are the descriptor segmentation experiment (Experiment 1), the optimal dual-scale descriptors threshold reference experiment (Experiment 2), and the ODSFD facade segmentation experiment (Experiment 3). Experiment 1 is used to select the optimal dual-scale descriptors, Experiment 2 is used to determine the threshold reference values of the optimal dual-scale descriptors, and Experiment 3 is used to verify the ODSFD algorithm's ability in facade segmentation. In each experiment, we conducted a detailed analysis of the results. Next, we will introduce these three experiments separately.

### 3.1. Descriptor Segmentation Experiment

#### 1) Experimental data

To find the optimal dual-scale feature descriptors that distinguish between regular and sharp points, it is necessary to evaluate the segmentation capabilities of each descriptor. We selected three sets of data for the experiments, which come from the Semantic 3D public dataset and synthetic data. Two sets of measured data come from Semantic 3D, and one set is synthetic data. The synthetic data is generated based on model, so the point distribution is relatively regular. The three sets of data are named Shice\_1, Shice\_2, and Moni\_1. The schematic diagram and detailed information of the three sets of data are shown in **Figure 3** and **Table 2**, respectively.

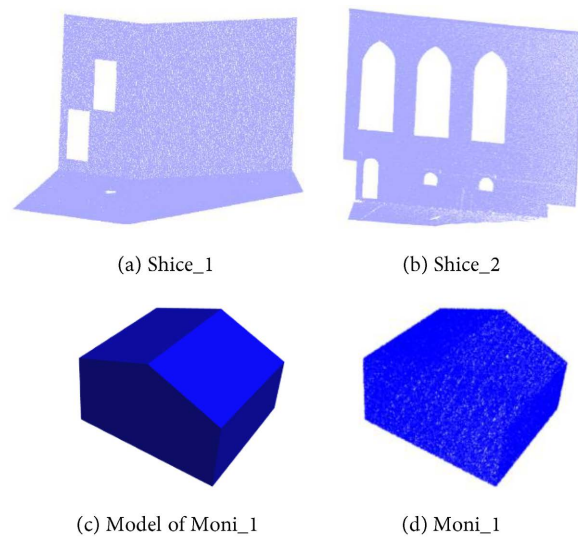


**Figure 3.** The diagram of datasets in experiment 1.

**Table 2.** Detailed information of datasets.

Data	Source	Number of point ploud
Shice_1	Semantic 3D domfountain3	544,298
Shice_2	Semantic 3D sg28_4	202,744
Moni_1	Reference []	30,300

#### 2) Evaluation metrics

We use Precision, Recall, and F1 score as evaluation metrics for the experimental results. The expressions for these three metrics are as Equations (3)-(5):

$$\text{Precision} = \frac{TP}{TP + FP} . \quad (3)$$

$$\text{Recall} = \frac{TP}{TP + FN} . \quad (4)$$

$$\text{F1-Score} = 2 * \frac{\text{Recall} * \text{Precision}}{\text{Recall} + \text{Precision}} . \quad (5)$$

where, TP (True Positives) is the number of correctly classified sharp points; FP (False Positives) is the number of regular points incorrectly classified as sharp; FN (False Negatives) is the number of sharp points incorrectly classified as regular.

### 3) Experimental methodology

We categorize the point clouds within the scene into two classes: sharp points and regular points. To intuitively analyze the segmentation capabilities of various feature descriptors, we use the RF (Random Forest) algorithm for data classification. We calculate the classification results of single descriptor, dual-scale descriptors combining any two descriptors, and multi-scale descriptors, and select the optimal dual-scale descriptors based on the classification results. For the reference datasets, sharp points extracted by manually adjusting the angle threshold parameter of RG are used as the standard values for sharp points, while the remaining points are used as the standard values for regular points. The segmentation results of the standard datasets are shown in **Figure 4**.

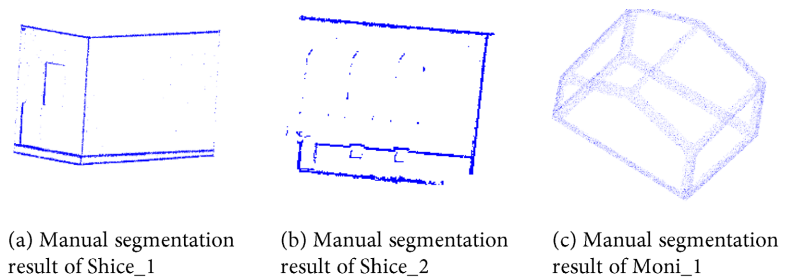


**Figure 4.** The segmentation results of the standard datasets.

Regarding the RF parameter settings, due to the significant difference in the number of regular and sharp points, we aim to reduce the impact of different class data sizes on the classification results. For each of the three datasets, we manually select 4000 sharp points and  $n * 4000$  regular points as the training dataset to ensure a uniform ratio of each class in the dataset (where  $n$  is the ratio of regular points to sharp points obtained from the reference dataset). Additionally, we select 30% of the points from the training set as the test set to analyze the classification ability of the descriptors.

The number of decision trees and the minimum number of leaf nodes also affect the algorithm's complexity and accuracy. We set the number of decision trees to 100 and the minimum number of leaf nodes to 5, considering both classification accuracy and computational complexity.

### 4) Results and analysis

**Figure 5** displays the classification results of three datasets when considering both single descriptor and all combinations of dual-scale descriptors. The results are presented in the form of a score matrix, where the diagonal elements represent the classification results of the single descriptor.

The experimental results indicate that compared to single descriptor, dual-scale descriptors show significant improvements in Precision, Recall, and

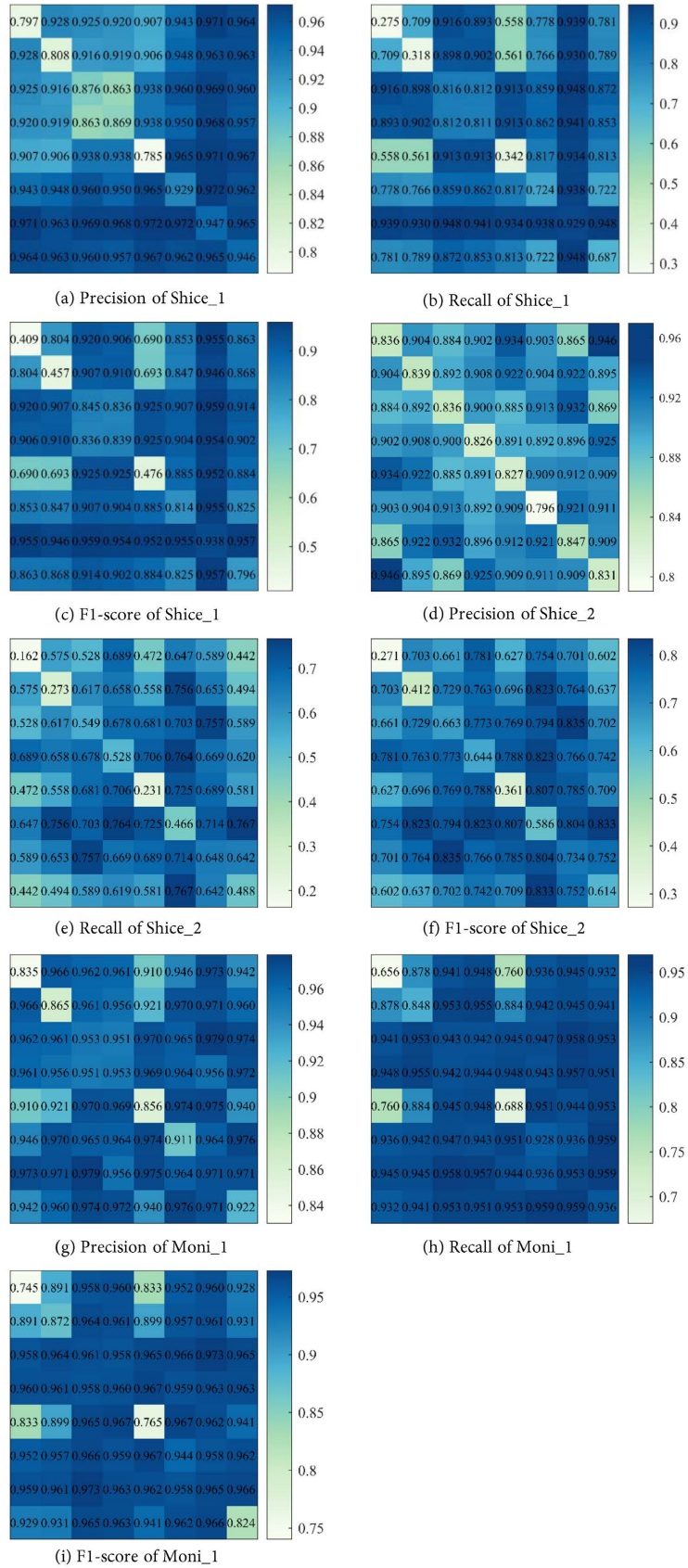


Figure 5. The classification results of datasets.

F1-score, demonstrating the effectiveness of the proposed method. Among all dual-scale descriptor combinations, the combination of feature descriptor  $S_{\text{sphericity}}$  and feature descriptor  $S_{\text{surface\_variation}}$  performs the best in terms of F1-score (0.959, 0.835, and 0.973 respectively) and achieves the best Precision in Moni\_1 (0.988). For the Shice\_1, this combination achieves a Precision of 0.969, which, although not the highest among all combinations, is only 0.003 lower than the highest Precision of 0.972. Therefore, we select  $S_{\text{sphericity}}$  and  $S_{\text{surface\_variation}}$  as the optimal dual-scale feature descriptors.

**Table 3** presents the detailed classification results for the three datasets using single feature descriptor, optimal dual-scale feature descriptors, and all descriptors considered.

**Table 3.** Detailed classification results for datasets.

$L_{\text{linearity}}$								
Data	SP number	RP number	TP	FP	FN	Precision	Recall	F1-score
Shice_1	1200	31200	330	84	870	0.797	0.275	0.409
Shice_2	1200	33600	194	38	1006	0.836	0.162	0.271
Moni_1	1200	3360	787	125	413	0.863	0.656	0.745
$P_{\text{planarity}}$								
Data	SP number	RP number	TP	FP	FN	Precision	Recall	F1-score
Shice_1	1200	31200	382	91	818	0.808	0.318	0.457
Shice_2	1200	33600	328	63	872	0.839	0.273	0.412
Moni_1	1200	3360	1017	116	183	0.898	0.848	0.872
$S_{\text{sphericity}}$								
Data	SP number	RP number	TP	FP	FN	Precision	Recall	F1-score
Shice_1	1200	31200	979	139	221	0.876	0.816	0.845
Shice_2	1200	33600	659	129	541	0.836	0.549	0.663
Moni_1	1200	3360	1131	23	69	<b>0.980</b>	0.943	0.961
$A_{\text{anisotropy}}$								
Data	SP number	RP number	TP	FP	FN	Precision	Recall	F1-score
Shice_1	1200	31200	973	147	227	0.869	0.811	0.839
Shice_2	1200	33600	634	134	566	0.826	0.528	0.644
Moni_1	1200	3360	1133	27	67	0.977	0.944	0.960
$E_{\text{eigenentropy}}$								
Data	SP number	RP number	TP	FP	FN	Precision	Recall	F1-score
Shice_1	1200	31200	410	112	790	0.785	0.342	0.476
Shice_2	1200	33600	277	58	923	0.827	0.231	0.361
Moni_1	1200	3360	825	131	375	0.863	0.688	0.765

## Continued

$O_{\text{ominvariance}}$								
Data	SP number	RP number	TP	FP	FN	Precision	Recall	F1-score
Shice_1	1200	31200	869	66	331	0.929	0.724	0.814
Shice_2	1200	33600	559	144	641	0.796	0.466	0.586
Moni_1	1200	3360	1114	46	86	0.960	0.928	0.944
$S_{\text{urface\_variation}}$								
Data	SP number	RP number	TP	FP	FN	Precision	Recall	F1-score
Shice_1	1200	31200	1115	63	85	<b>0.947</b>	<b>0.929</b>	<b>0.938</b>
Shice_2	1200	33600	778	141	422	<b>0.847</b>	<b>0.648</b>	<b>0.734</b>
Moni_1	1200	3360	1144	27	56	0.977	<b>0.953</b>	<b>0.965</b>
$V_{\text{verticality}}$								
Data	SP number	RP number	TP	FP	FN	Precision	Recall	F1-score
Shice_1	1200	31200	824	47	376	0.946	0.687	0.796
Shice_2	1200	33600	585	119	615	0.831	0.488	0.614
Moni_1	1200	3360	1123	107	77	0.913	0.936	0.824
$S_{\text{sphericity}} + S_{\text{urface\_variation}}$								
Data	SP number	RP number	TP	FP	FN	Precision	Recall	F1-score
Shice_1	1200	31200	1138	41	62	0.965	0.948	0.957
Shice_2	1200	33600	908	66	292	0.932	0.757	0.835
Moni_1	1200	3360	1150	14	50	0.988	0.958	0.973
$L_{\text{inearity}} + P_{\text{planarity}} + S_{\text{sphericity}} + A_{\text{anisotropy}} + E_{\text{eigenentropy}} + O_{\text{ominvariance}} + S_{\text{urface\_variation}} + V_{\text{verticality}}$								
Data	SP number	RP number	TP	FP	FN	Precision	Recall	F1-score
Shice_1	1200	31200	1154	29	46	0.976	0.962	0.969
Shice_2	1200	33600	940	47	260	0.952	0.784	0.860
Moni_1	1200	3360	1161	14	39	0.990	0.968	0.978

The results from **Table 3** indicate that, for all three datasets, single descriptors exhibit significantly lower Precision, Recall, and F1-scores compared to the selected optimal dual-scale descriptors. Specifically, for Shice\_1, the optimal dual-scale descriptors improve Precision by 0.018, Recall by 0.019, and F1-score by 0.019 compared to the highest single-scale descriptor values. For Shice\_2, the improvements are 0.085 in Precision, 0.109 in Recall, and 0.101 in F1-score. For Moni\_1, the improvements are 0.008 in Precision, 0.005 in Recall, and 0.008 in F1-score.

The improvements for the three metrics are significant for the measured data, with Shice\_2 showing a F1-score improvement of nearly 12%, while the im-

improvements are smaller for the simulated data. This is because the simulated data is more regular and has uniform point density, leading to good classification results for both single and dual-scale descriptors. However, in practical data collection processes, point clouds density is often uneven. Therefore, in terms of practical application considerations, this experiment also demonstrates that the optimal dual-scale descriptors obtained through this method have higher practical value.

Compared to the scenario where all eight descriptors are considered, the optimal dual-scale descriptors show slightly lower Precision, Recall, and F1-scores. Specifically, for Shice\_1, the multi-scale descriptors improve Precision by 0.011, Recall by 0.014, and F1-score by 0.012 compared to the optimal dual-scale descriptors. For Shice\_2, the multi-scale descriptors improve Precision by 0.002, Recall by 0.027, and F1-score by 0.025. For Moni\_1, Precision improves by 0.002, Recall by 0.010, and F1-score by 0.005.

Although the multi-scale descriptors show improvements in all three metrics, the improvements are not significant for both measured and simulated data, while the computational complexity increases significantly. In the implementation of the algorithm, suitable parameters need to be provided for all eight descriptors, whereas the dual-scale descriptors only require two parameters. In conclusion, the proposed dual-scale descriptors greatly reduce the computational cost with a minor sacrifice in segmentation accuracy. Subsequent experiments will analyze the distribution of  $S_{\text{sphericity}}$  and  $S_{\text{surface\_variation}}$  values for regular and sharp points and provide reference thresholds.

### 3.2. Optimal Dual-Scale Descriptors Threshold Reference Experiment

#### 1) Experimental data

To obtain more generalizable reference thresholds for distinguishing sharp points from regular points, the same three datasets used in Experiment 3.1 were employed in this experiment.

#### 2) Results and analysis

Compute the  $S_{\text{sphericity}}$  and  $S_{\text{surface\_variation}}$  values for regular and sharp points in the standard datasets of the three groups of data, and arrange the  $S_{\text{sphericity}}$  and  $S_{\text{surface\_variation}}$  values of the two types of points in ascending order. The resulting curve is shown in **Figure 6**, where the  $x$ -axis represents the point number and the  $y$ -axis represents the  $S_{\text{sphericity}}$  and  $S_{\text{surface\_variation}}$  values for each point.

From **Figure 6**, we can see that the  $S_{\text{sphericity}}$  and  $S_{\text{surface\_variation}}$  values of regular and sharp points in the three datasets exhibit similar distribution trends for the dual-scale descriptors values. In both the measured and simulated data, the majority of regular points have low  $S_{\text{sphericity}}$  and  $S_{\text{surface\_variation}}$  values, close to 0, with only about 1% of regular points having relatively high  $S_{\text{sphericity}}$  and  $S_{\text{surface\_variation}}$  values. Similarly, the majority of sharp points have high  $S_{\text{sphericity}}$  and  $S_{\text{surface\_variation}}$  values. For Shice\_1 and Shice\_2, only about 5% of sharp points have  $S_{\text{sphericity}}$  values less than 0.02 and  $S_{\text{surface\_variation}}$  values less than 0.01, while in Moni\_1, only

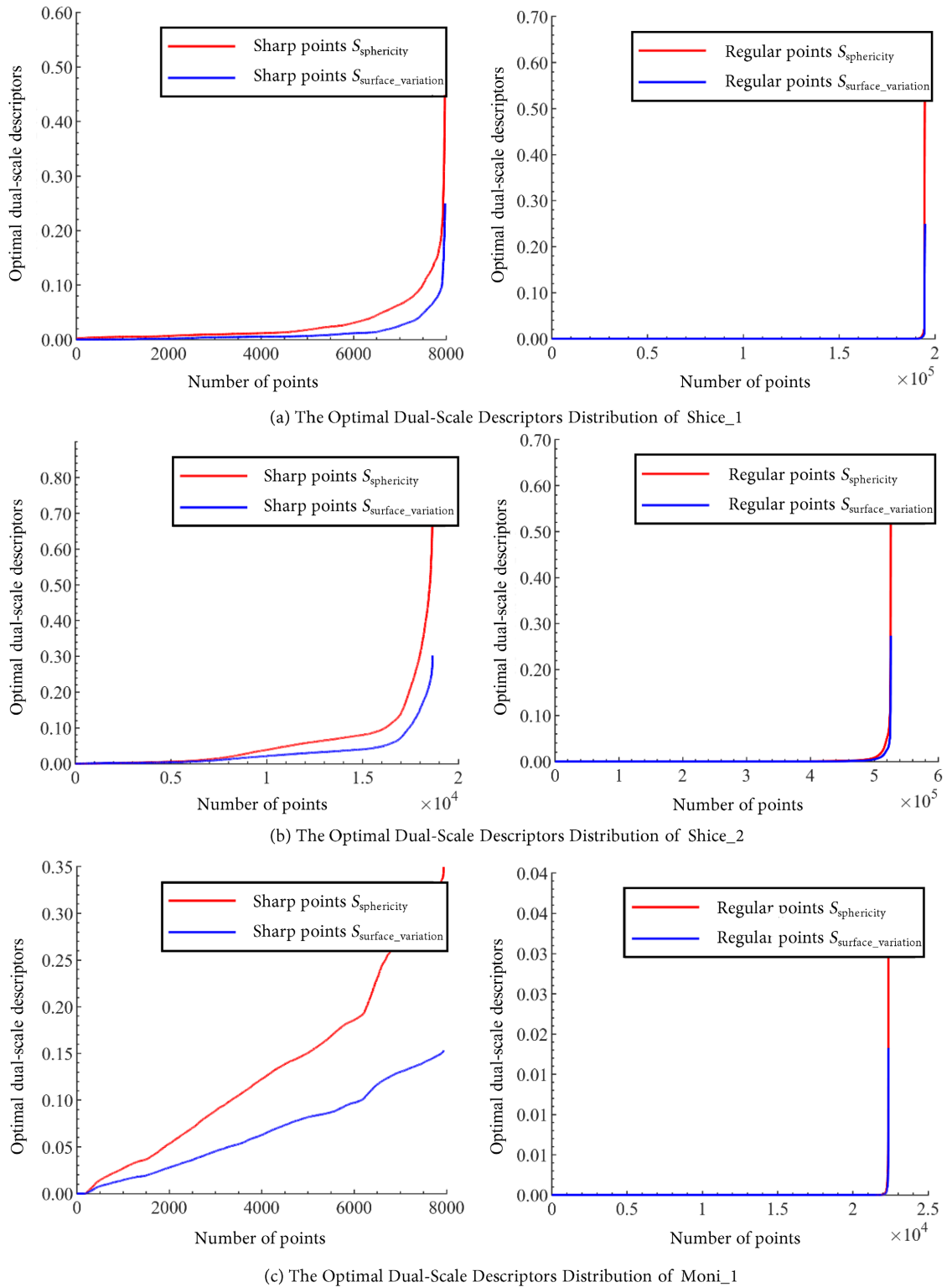


**Figure 6.** The distribution of  $S_{sphericity}$  and  $S_{surface\_variation}$ .

about 1% of sharp points have  $S_{sphericity}$  values less than 0.02 and  $S_{surface\_variation}$  values less than 0.01. The 1% or 5% discrepancy in regular and sharp points could be attributed to two reasons. Firstly, it could be due to errors in the standard da-

tasets themselves, as the classification of regular and sharp points in the standard datasets is determined by manually adjusting the normal vector angle threshold, which may introduce some human error. Secondly, it could be due to suboptimal radius settings for computing the feature values of some points, leading to errors in the computed feature values and further affecting the calculation of the feature descriptors.

From these three sets of data, it can be seen that effective differentiation between regular and sharp points can be achieved when the  $S_{\text{sphericity}}$  threshold is set to 0.02 and the  $S_{\text{surface\_variation}}$  threshold is set to 0.01.

### 3.3. ODSFD Facade Segmentation Experiment

#### 1) Experimental data

The experimental data in this experiment are from two facades of a library at a university in Shanghai, China. The data was acquired using a Riegl VZ-400 terrestrial laser scanner. Each facade consists of multiple planar segments of varying sizes. The two facades are named Face\_1 and Face\_2. The schematic diagrams of the two facades and detailed information about the point clouds data are shown in **Figure 7** and **Table 4**, respectively.

#### 2) Evaluation metrics

The evaluation metrics for the experiment are Precision, Recall, and F1-score.

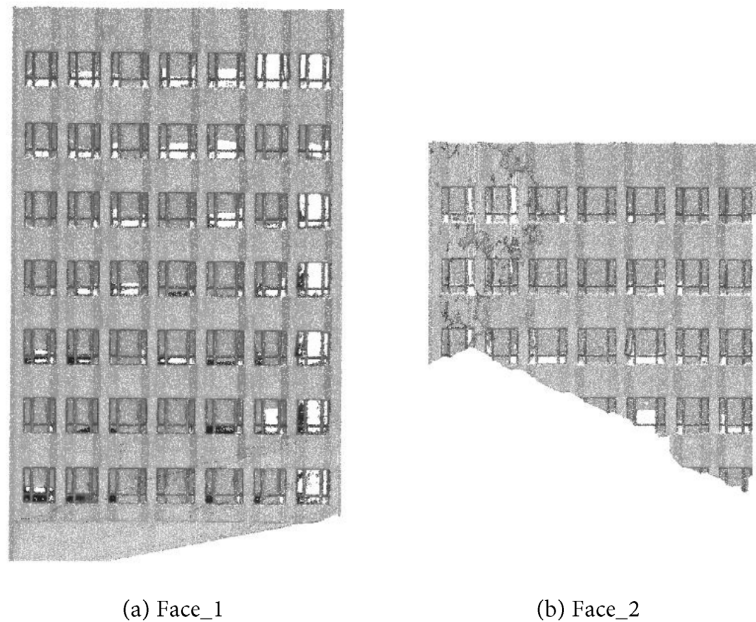


**Figure 7.** The schematic diagrams of the two facades.

**Table 4.** Detailed information of datasets.

Data	Source	Number of point clouds
Face_1	A library in China	431,746
Face_2	A library in China	183,210

### 3) Experimental methodology

In the segmentation process of the two facades, the  $S_{\text{sphericity}}$  and  $S_{\text{surface\_variation}}$  thresholds are set to 0.02 and 0.01, respectively. To validate the effectiveness and accuracy of ODSFD, we use manually segmented results as the standard dataset. We compare our method with RG algorithms (with normal vector angle thresholds of  $5^\circ$  and  $10^\circ$ ) and the RANSAC algorithm applied to the same two facades.

### 4) Results and analysis

The segmentation results of Face\_1 using the RG algorithm (with a normal vector angle threshold of  $5^\circ$ ), the RG algorithm (with a normal vector angle threshold of  $10^\circ$ ), and the RANSAC algorithm are shown in **Figures 8(a)-(c)**,

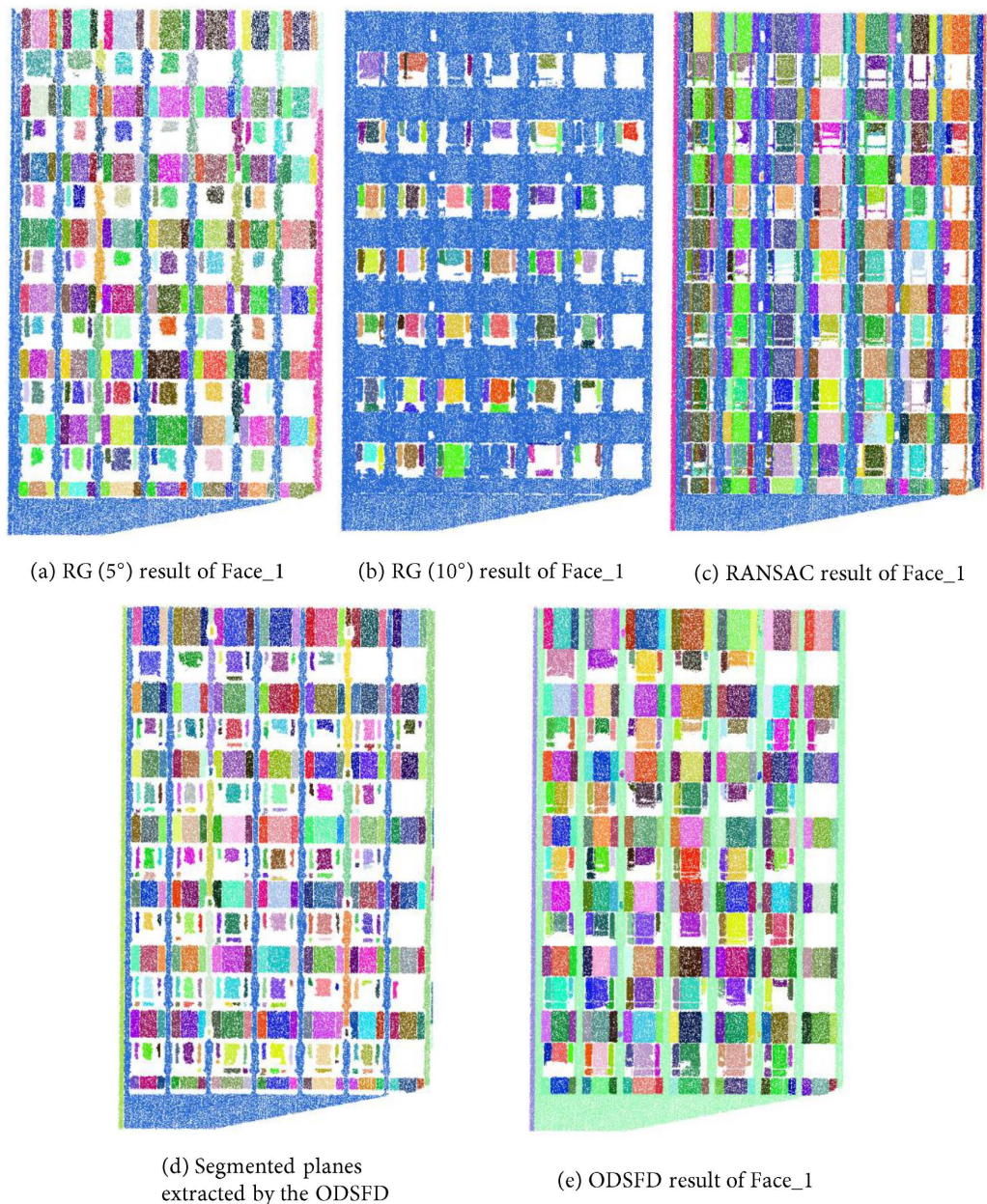


**Figure 8.** The segmentation results of Face\_1.

respectively. The segmented planes extracted by the ODSFD algorithm before optimization are shown in **Figure 8(d)**, with the results after optimization in **Figure 8(e)**. Similarly, for Face\_2, the segmentation results using the RG algorithm (with a normal vector angle threshold of  $5^\circ$ ), the RG algorithm (with a normal vector angle threshold of  $10^\circ$ ), and the RANSAC algorithm are shown in **Figures 9(a)-(c)**, respectively. The segmented planes extracted by the ODSFD algorithm before optimization are shown in **Figure 9(d)**, with the results after optimization in **Figure 9(e)**. The Precision, Recall, and F1-scores of the ODSFD algorithm and the comparison methods are summarized in **Table 5**.

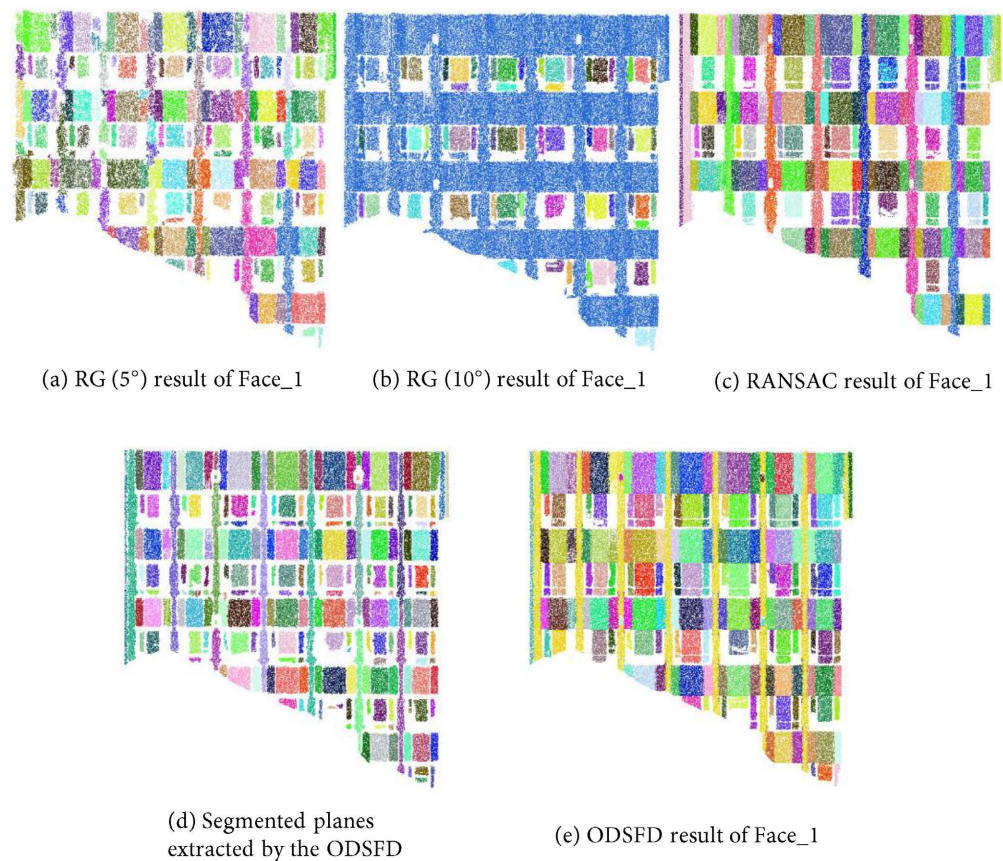


**Figure 9.** The segmentation results of Face\_2.

Analysis of **Table 5** reveals that the segmentation results of the traditional RG algorithm vary significantly depending on the normal vector angle threshold. A smaller angle threshold results in a higher number of segmented planes. For Face\_1, the traditional RG algorithm with a  $5^\circ$  threshold segmented 243 planes, while the  $10^\circ$  threshold resulted in only 102 planes. Similarly, for Face\_2, the  $5^\circ$  threshold yielded 157 planes, whereas the  $10^\circ$  threshold produced just 59 planes. Both thresholds exhibited varying degrees of over-segmentation, under-segmentation, and missed segmentation. The RANSAC algorithm's segmentation capability was between the traditional RG algorithms with  $5^\circ$  and  $10^\circ$  thresholds, segmenting 210 planes for Face\_1 and 124 planes for Face\_2, but still showed issues of

**Table 5.** The segmentation results of ODSFD and comparison methods.

Face_1	RG (5°)	RG (10°)	RANSAC	Before optimization	ODSFD
Manual	304	304	304	304	304
Number of segmented planes	243	102	210	378	302
over-segmentation	14	7	3	76	0
under-segmentation	11	1	25	0	0
missed-segmentation	66	178	41	2	2
Precision	0.897	0.922	0.867	0.799	1
Recall	0.717	0.309	0.599	0.993	0.993
F1-score	0.797	0.463	0.709	0.885	0.996
Face_2					
Manual	163	163	163	163	163
Number of segmented planes	157	59	124	219	162
over-segmentation	22	4	0	57	0
under-segmentation	19	2	1	0	0
missed-segmentation	16	16	47	1	1
Precision	0.739	0.898	0.992	0.740	1
Recall	0.712	0.325	0.755	0.994	0.994
F1-score	0.725	0.477	0.857	0.848	0.997

over-segmentation, under-segmentation, and missed segmentation.

In terms of Precision, Recall, and F1-score, the ODSFD algorithm outperformed the other methods. For Face\_1, the ODSFD algorithm achieved a Precision of 1, a Recall of 0.993, and an F1-score of 0.996. Compared to the other three methods, the ODSFD algorithm's Precision improved by 0.103, 0.078, and 0.133, respectively; Recall improved by 0.276, 0.684, and 0.394, respectively; and the F1-score improved by 0.199, 0.533, and 0.287, respectively. The results for Face\_2 were similar, with the ODSFD algorithm also achieving the best segmentation results.

From the pre-optimization results of the ODSFD, it is evident that while over-segmentation was severe, resulting in a number of segmented planes far exceeding the actual number of planes. However, post-optimization, the number of over-segmented planes significantly decreased, demonstrating the effectiveness of the proposed optimization method.

For Face\_1, the ODSFD resulted in two missed planes, while Face\_2 had one missed plane. This can be attributed to two main reasons: firstly, the quality of the point clouds data for these planes was relatively low, and secondly, the sur-

faces of these planes were highly undulating, making them more like curved surfaces than flat planes.

#### 4. Conclusion

We focused on building facades as our research subject and proposed an ODSFD facade point clouds segmentation method based on optimal dual-scale feature descriptors by thoroughly exploring the geometric feature information of facade point clouds. First, we selected the optimal dual-scale descriptors through experiments to construct the segmentation algorithm. Then, we provided more general threshold reference values based on the distribution of descriptors. Finally, we validated the feasibility of the proposed ODSFD algorithm using measured data. From the final comparative experiments, the ODSFD algorithm demonstrated more accurate segmentation results. It was able to produce multiple fine-grained planes even for relatively complex building facades. However, the ODSFD algorithm still has shortcomings, notably severe over-segmentation before optimization, which increases the computational cost of subsequent optimizations. Additionally, the threshold reference values for the optimal dual-scale descriptors were derived from only three datasets. In the future, we plan to use more datasets to provide more convincing and accurate threshold reference values.

#### Acknowledgements

We are very grateful for the support of the National Natural Science Foundation of China (42074022) for our research.

#### Conflicts of Interest

The authors declare no conflicts of interest regarding the publication of this paper.

#### References

- [1] Pantoja-Rosero, B.G., Achanta, R., Kozinski, M., Fua, P., Perez-Cruz, F. and Beyer, K. (2022) Generating LoD3 Building Models from Structure-from-Motion and Semantic Segmentation. *Automation in Construction*, **141**, Article ID: 104430. <https://doi.org/10.1016/j.autcon.2022.104430>
- [2] Chen, Z., Ledoux, H., Khademi, S. and Nan, L. (2022) Reconstructing Compact Building Models from Point Clouds Using Deep Implicit Fields. *ISPRS Journal of Photogrammetry and Remote Sensing*, **194**, 58-73. <https://doi.org/10.1016/j.isprsjprs.2022.09.017>
- [3] Nan, L. and Wonka, P. (2017) Polyfit: Polygonal Surface Reconstruction from Point Clouds. *Proceedings of the 16th International Conference on Computer Vision*, Venice, 22-29 October 2017, 258. <https://doi.org/10.1109/iccv.2017.258>
- [4] Rabbani, T., Heuvel, F.A. and Vosselman, G. (2006) Segmentation of Point Clouds Using Smoothness Constraint. *Proceedings of the ISPRS Commission V Symposium "Image Engineering and Vision Metrology"*, Aalborg, 15-17 May 2006, 248-253.
- [5] Yu, B., Hu, J., Dong, X., Dai, K., Xiao, D., Zhang, B., *et al.* (2022) A Robust Automatic Method to Extract Building Facade Maps from 3D Point Cloud Data. *Remote*

- Sensing*, **14**, Article No. 3848. <https://doi.org/10.3390/rs14163848>
- [6] Lin, Y., Li, J., Wang, C., Chen, Z., Wang, Z. and Li, J. (2020) Fast Regularity-Constrained Plane Fitting. *ISPRS Journal of Photogrammetry and Remote Sensing*, **161**, 208-217. <https://doi.org/10.1016/j.isprsjprs.2020.01.009>
- [7] Lu, X., Xing, K., Liu, R. and Wang, P. (2019) Gradual Segmentation Method for Building Facade in 3D Laser Point Clouds. *Science of Surveying and Mapping*, **44**, 7-13.
- [8] Yang, B., Dong, Z., Wei, Z., Fang, L. and Li, H. (2013) Extracting Complex Building Facades from Mobile Laser Scanning Data. *Acta Geodaetica et Cartographica Sinica*, **42**, 411-417.
- [9] Wang, Y., Hao, W., Ning, X., Zhao, M., Zhang, J., Shi, Z., et al. (2013) Automatic Segmentation of Urban Point Clouds Based on the Gaussian Map. *The Photogrammetric Record*, **28**, 342-361. <https://doi.org/10.1111/phor.12041>
- [10] Wang, W., Zhang, Y., Ge, G., Jiang, Q., Wang, Y. and Hu, L. (2023) Indoor Point Cloud Segmentation Using a Modified Region Growing Algorithm and Accurate Normal Estimation. *IEEE Access*, **11**, 42510-42520. <https://doi.org/10.1109/access.2023.3270709>
- [11] Jampani, V., Gadde, R. and Gehler, P.V. (2015) Efficient Facade Segmentation Using Auto-Context. *Proceedings of the IEEE Winter Conference on Applications of Computer Vision*, Hawaii, 5-9 January 2015, 1038-1045. <https://doi.org/10.1109/wacv.2015.143>
- [12] Hackel, T., Wegner, J.D. and Schindler, K. (2016) Contour Detection in Unstructured 3D Point Clouds. *Proceedings of the International Conference on Computer Vision and Pattern Recognition*, Las Vegas, 26-30 June 2016, 178. <https://doi.org/10.1109/cvpr.2016.178>
- [13] Zhang, L., Guo, J., Cheng, Z., Xiao, J. and Zhang, X. (2022) Efficient Pairwise 3-D Registration of Urban Scenes via Hybrid Structural Descriptors. *IEEE Transactions on Geoscience and Remote Sensing*, **60**, 1-17. <https://doi.org/10.1109/tgrs.2021.3091380>
- [14] Hoppe, H., DeRose, T., Duchamp, T., McDonald, J. and Stuetzle, W. (1992) Surface Reconstruction from Unorganized Points. *Proceedings of the 19th ACM SIGGRAPH Computer Graphics*, Vol. 26, 71-78. <https://doi.org/10.1145/142920.134011>
- [15] Gholinejad, S., Amiri-Simkooei, A., Alizadeh Moghaddam, S.H. and Alizadeh Naeini, A. (2020) An Automated PCA-Based Approach towards Optimization of the Rational Function Model. *ISPRS Journal of Photogrammetry and Remote Sensing*, **165**, 133-139. <https://doi.org/10.1016/j.isprsjprs.2020.05.011>
- [16] Pauly, M., Keiser, R. and Gross, M. (2003) Multi-Scale Feature Extraction on Point-Sampled Surfaces. *Computer Graphics Forum*, **22**, 281-289. <https://doi.org/10.1111/1467-8659.00675>
- [17] Canaz Sevgen, S. and Karsli, F. (2019) An Improved RANSAC Algorithm for Extracting Roof Planes from Airborne Lidar Data. *The Photogrammetric Record*, **35**, 40-57. <https://doi.org/10.1111/phor.12296>
- [18] Li, Z. and Shan, J. (2022) RANSAC-Based Multi Primitive Building Reconstruction from 3D Point Clouds. *ISPRS Journal of Photogrammetry and Remote Sensing*, **185**, 247-260. <https://doi.org/10.1016/j.isprsjprs.2021.12.012>
- [19] Xie, T., Chen, H., Liu, W., Zhou, R. and Li, Q. (2024) 3D Surface Segmentation from Point Clouds via Quadric Fits Based on DBSCAN Clustering. *Pattern Recognition*, **154**, Article ID: 110589. <https://doi.org/10.1016/j.patcog.2024.110589>

- [20] Czerniawski, T., Sankaran, B., Nahangi, M., Haas, C. and Leite, F. (2018) 6D DBSCAN-Based Segmentation of Building Point Clouds for Planar Object Classification. *Automation in Construction*, **88**, 44-58.  
<https://doi.org/10.1016/j.autcon.2017.12.029>